

Measurement of ϕ_3 with Dalitz Plot Analysis of $B^\pm \rightarrow D^{(*)}K^\pm$ Decay

A. Poluektov,¹ K. Abe,⁷ T. Abe,⁷ H. Aihara,⁴² Y. Asano,⁴⁶ T. Aushev,¹¹ T. Aziz,³⁸ S. Bahinipati,⁴ A. M. Bakich,³⁷ I. Bedny,¹ U. Bitenc,¹² I. Bizjak,¹² S. Blyth,²⁴ A. Bondar,¹ A. Bozek,²⁵ M. Bračko,^{18,12} J. Brodzicka,²⁵ T. E. Browder,⁶ P. Chang,²⁴ Y. Chao,²⁴ B. G. Cheon,³ R. Chistov,¹¹ S.-K. Choi,⁵ Y. Choi,³⁶ A. Chuvikov,³² M. Danilov,¹¹ M. Dash,⁴⁷ L. Y. Dong,⁹ S. Eidelman,¹ V. Eiges,¹¹ Y. Enari,²⁰ S. Fratina,¹² N. Gabyshev,¹ A. Garmash,³² T. Gershon,⁷ G. Gokhroo,³⁸ B. Golob,^{17,12} R. Guo,²² J. Haba,⁷ T. Hara,²⁹ K. Hayasaka,²⁰ H. Hayashii,²¹ M. Hazumi,⁷ T. Higuchi,⁷ L. Hinz,¹⁶ T. Hokuue,²⁰ Y. Hoshi,⁴⁰ W.-S. Hou,²⁴ Y. B. Hsiung,^{24,*} A. Imoto,²¹ K. Inami,²⁰ A. Ishikawa,⁷ R. Itoh,⁷ H. Iwasaki,⁷ M. Iwasaki,⁴² J. H. Kang,⁴⁸ J. S. Kang,¹⁴ S. U. Kataoka,²¹ N. Katayama,⁷ H. Kawai,² T. Kawasaki,²⁷ H. R. Khan,⁴³ H. J. Kim,¹⁵ J. H. Kim,³⁶ S. K. Kim,³⁵ K. Kinoshita,⁴ P. Koppenburg,⁷ S. Korpar,^{18,12} P. Križan,^{17,12} P. Krokovny,¹ A. Kuzmin,¹ Y.-J. Kwon,⁴⁸ S. H. Lee,³⁵ T. Lesiak,²⁵ J. Li,³⁴ S.-W. Lin,²⁴ J. MacNaughton,¹⁰ F. Mandl,¹⁰ D. Marlow,³² T. Matsumoto,⁴⁴ A. Matyja,²⁵ W. Mitaroff,¹⁰ K. Miyabayashi,²¹ H. Miyata,²⁷ R. Mizuk,¹¹ T. Mori,⁴³ T. Nagamine,⁴¹ Y. Nagasaka,⁸ T. Nakadaira,⁴² M. Nakao,⁷ H. Nakazawa,⁷ Z. Natkaniec,²⁵ S. Nishida,⁷ O. Nitoh,⁴⁵ T. Nozaki,⁷ S. Ogawa,³⁹ T. Ohshima,²⁰ T. Okabe,²⁰ S. Okuno,¹³ S. L. Olsen,⁶ W. Ostrowicz,²⁵ H. Ozaki,⁷ P. Pakhlov,¹¹ N. Parslow,³⁷ L. E. Piilonen,⁴⁷ N. Root,¹ M. Rozanska,²⁵ H. Sagawa,⁷ S. Saitoh,⁷ Y. Sakai,⁷ T. R. Sarangi,⁷ N. Sato,²⁰ O. Schneider,¹⁶ J. Schümann,²⁴ C. Schwanda,¹⁰ A. J. Schwartz,⁴ S. Semenov,¹¹ K. Senyo,²⁰ R. Seuster,⁶ M. E. Sevir,¹⁹ H. Shibuya,³⁹ B. Shwartz,¹ V. Sidorov,¹ A. Somov,⁴ N. Soni,³⁰ R. Stamen,⁷ S. Stanič,^{46,†} M. Starič,¹² A. Sugiyama,³³ K. Sumisawa,²⁹ T. Sumiyoshi,⁴⁴ S. Suzuki,³³ O. Tajima,⁴¹ F. Takasaki,⁷ K. Tamai,⁷ N. Tamura,²⁷ M. Tanaka,⁷ G. N. Taylor,¹⁹ Y. Teramoto,²⁸ K. Trabelsi,⁶ T. Tsuboyama,⁷ T. Tsukamoto,⁷ S. Uehara,⁷ T. Uglov,¹¹ K. Ueno,²⁴ Y. Unno,² S. Uno,⁷ G. Varner,⁶ K. E. Varvell,³⁷ S. Villa,¹⁶ C. H. Wang,²³ M.-Z. Wang,²⁴ M. Watanabe,²⁷ B. D. Yabsley,⁴⁷ Y. Yamada,⁷ A. Yamaguchi,⁴¹ Y. Yamashita,²⁶ M. Yamauchi,⁷ J. Ying,³¹ Y. Yusa,⁴¹ S. L. Zang,⁹ J. Zhang,⁷ Z. P. Zhang,³⁴ V. Zhilich,¹ D. Žontar,^{17,12} and D. Zürcher¹⁶

(The Belle Collaboration)

¹*Budker Institute of Nuclear Physics, Novosibirsk*

²*Chiba University, Chiba*

³*Chonnam National University, Kwangju*

⁴*University of Cincinnati, Cincinnati, Ohio 45221*

⁵*Gyeongsang National University, Chinju*

⁶*University of Hawaii, Honolulu, Hawaii 96822*

⁷*High Energy Accelerator Research Organization (KEK), Tsukuba*

⁸*Hiroshima Institute of Technology, Hiroshima*

⁹*Institute of High Energy Physics, Chinese Academy of Sciences, Beijing*

¹⁰*Institute of High Energy Physics, Vienna*

¹¹*Institute for Theoretical and Experimental Physics, Moscow*

¹²*J. Stefan Institute, Ljubljana*

¹³*Kanagawa University, Yokohama*

¹⁴*Korea University, Seoul*

¹⁵*Kyungpook National University, Taegu*

¹⁶*Swiss Federal Institute of Technology of Lausanne, EPFL, Lausanne*

¹⁷*University of Ljubljana, Ljubljana*

¹⁸*University of Maribor, Maribor*

¹⁹*University of Melbourne, Victoria*

²⁰*Nagoya University, Nagoya*

²¹*Nara Women's University, Nara*

²²*National Kaohsiung Normal University, Kaohsiung*

²³*National United University, Miao Li*

²⁴*Department of Physics, National Taiwan University, Taipei*

²⁵*H. Niewodniczanski Institute of Nuclear Physics, Krakow*

²⁶*Nihon Dental College, Niigata*

²⁷*Niigata University, Niigata*

²⁸*Osaka City University, Osaka*

²⁹*Osaka University, Osaka*

³⁰*Panjab University, Chandigarh*

³¹*Peking University, Beijing*

³²*Princeton University, Princeton, New Jersey 08545*

³³*Saga University, Saga*

³⁴*University of Science and Technology of China, Hefei*

³⁵Seoul National University, Seoul

³⁶Sungkyunkwan University, Suwon

³⁷University of Sydney, Sydney NSW

³⁸Tata Institute of Fundamental Research, Bombay

³⁹Toho University, Funabashi

⁴⁰Tohoku Gakuin University, Tagajo

⁴¹Tohoku University, Sendai

⁴²Department of Physics, University of Tokyo, Tokyo

⁴³Tokyo Institute of Technology, Tokyo

⁴⁴Tokyo Metropolitan University, Tokyo

⁴⁵Tokyo University of Agriculture and Technology, Tokyo

⁴⁶University of Tsukuba, Tsukuba

⁴⁷Virginia Polytechnic Institute and State University, Blacksburg, Virginia 24061

⁴⁸Yonsei University, Seoul

We present a measurement of the unitarity triangle angle ϕ_3 using a Dalitz plot analysis of the three-body decay of the neutral D meson from the $B^\pm \rightarrow D^{(*)}K^\pm$ process. The method employs the interference between D^0 and \bar{D}^0 to extract both the weak and strong phases. We apply this method to a 140 fb^{-1} data sample collected by the Belle experiment. The analysis uses the modes $B^\pm \rightarrow DK^\pm$ and $B^\pm \rightarrow D^*K^\pm$, $D^* \rightarrow D\pi^0$, where the neutral D meson decays into $K_S\pi^+\pi^-$. We obtain 146 signal candidates for $B^\pm \rightarrow DK^\pm$ and 39 candidates for $B^\pm \rightarrow D^*K^\pm$. From a combined maximum likelihood fit to the $B^\pm \rightarrow DK^\pm$ and $B^\pm \rightarrow D^*K^\pm$ modes, we obtain $\phi_3 = 77^\circ_{-19^\circ}^{+17^\circ}(\text{stat}) \pm 13^\circ(\text{syst}) \pm 11^\circ(\text{model})$. The corresponding two standard deviation interval is $26^\circ < \phi_3 < 126^\circ$.

PACS numbers: 13.25.Hw, 14.40.Nd

INTRODUCTION

Determinations of the Cabibbo-Kobayashi-Maskawa (CKM) [1] matrix elements provide important checks on the consistency of the Standard Model and ways to search for new physics. The possibility of observing direct CP violation in $B \rightarrow DK$ decays was first discussed by I. Bigi and A. Sanda [2]. Since then, various methods using CP violation in $B \rightarrow DK$ decays have been proposed [3] to measure the unitarity triangle angle ϕ_3 . These methods are based on two key observations: neutral D^0 and \bar{D}^0 mesons can decay to a common final state, and the decay $B^+ \rightarrow D^{(*)}K^+$ can produce neutral D mesons of both flavors via $\bar{b} \rightarrow \bar{c}u\bar{s}$ (Fig. 1a) and $\bar{b} \rightarrow \bar{u}c\bar{s}$ (Fig. 1b) transitions, with the relative phase θ_+ between the two interfering amplitudes that is the sum, $\delta + \phi_3$, of strong and weak interaction phases. For the charge conjugate mode, the relative phase is $\theta_- = \delta - \phi_3$, so both phases can be extracted from measurements of such charge conjugate B decay modes.

The data samples accumulated by currently running experiments are not yet sufficiently large to constrain the value of ϕ_3 with reasonable significance. A novel technique based on the analysis of three body decays of the neutral D meson has been proposed [4], which has a higher statistical precision than methods based on branching fraction measurements. In this case, the measurement is based on the analysis of the Dalitz distribution of three body final states common to D^0 and \bar{D}^0 , such as $K_S\pi^+\pi^-$.

In the Wolfenstein parameterization of the CKM matrix elements, the amplitudes of the two diagrams that contribute to the decay $B^+ \rightarrow DK^+$ are given by $M_1 \sim V_{cb}^*V_{us} \sim A\lambda^3$ (for the \bar{D}^0K^+ final state) and $M_2 \sim V_{ub}^*V_{cs} \sim A\lambda^3(\rho + i\eta)$ (for D^0K^+). The annihilation diagram also contributes to M_2 , but, since the weak coefficients are the same, this effectively leads to a redefinition of the strong phase. The two amplitudes M_1 and M_2 interfere as the D^0 and \bar{D}^0 mesons decay into the same final state $K_S\pi^+\pi^-$; we denote the admixed state as \tilde{D} . Assuming no CP asymmetry in neutral D decays, the amplitude of the B^+ decay can be written as

$$M_+ = f(m_+^2, m_-^2) + r e^{i\phi_3 + i\delta} f(m_-^2, m_+^2), \quad (1)$$

where m_+^2 and m_-^2 are the squared invariant masses of the $K_S\pi^+$ and $K_S\pi^-$ combinations, respectively, and $f(m_+, m_-)$ is the complex amplitude for the decay $\bar{D}^0 \rightarrow K_S\pi^+\pi^-$. The absolute value of the ratio between the two interfering amplitudes, r , is given by the ratio $|V_{ub}^*V_{cs}|/|V_{cb}^*V_{us}| \sim 0.38$ and the color suppression factor. The latter can be roughly estimated from the ratio of the color suppressed $\bar{B}^0 \rightarrow D^0\bar{K}^0$ [5] and color allowed $B^- \rightarrow D^0K^-$ decays [6]: $\sqrt{\mathcal{B}(\bar{B}^0 \rightarrow D^0\bar{K}^0)/\mathcal{B}(B^- \rightarrow D^0K^-)} = 0.35 \pm 0.05$. The amplitude ratio is therefore expected to be the product of these two factors, *i. e.* $r \sim 0.13$.

The corresponding amplitude for the charge conjugate B^- decay is

$$M_- = f(m_-^2, m_+^2) + r e^{-i\phi_3 + i\delta} f(m_+^2, m_-^2). \quad (2)$$

Once the functional form of f is fixed by a model for $\bar{D}^0 \rightarrow K_S \pi^+ \pi^-$, the \tilde{D} Dalitz distributions for B^+ and B^- decays can be fitted simultaneously using the above expressions for M_+ and M_- , with r , ϕ_3 , and δ as free parameters. There are certain advantages of this technique: it is directly sensitive to the value of ϕ_3 and does not require additional assumptions on the values of r and δ . Moreover, the value of r obtained in the fit can be useful for other ϕ_3 measurements.

Reference [4] suggests a model-independent way for determining ϕ_3 via a binned Dalitz plot analysis. However, the application of this procedure would result in large statistical errors with our present data sample. Instead, we use a model-dependent approach based on an unbinned maximum likelihood fit to the $\tilde{D} \rightarrow K_S \pi^+ \pi^-$ Dalitz plot distributions corresponding to B^+ and B^- data samples, thus making optimal use of our small number of signal events. The model of $\bar{D}^0 \rightarrow K_S \pi^+ \pi^-$ decay in our approach is determined from a large sample of flavor-tagged $\bar{D}^0 \rightarrow K_S \pi^+ \pi^-$ decays produced in continuum e^+e^- annihilation. The drawback of this approach is that only the absolute value of the D^0 decay amplitude f can be determined directly; the complex form of f has to be based on model assumptions; these lead to potential model-dependent uncertainties in the determination of ϕ_3 . Note, however, that the model uncertainties can be controlled in the future using data from τ -charm factories. CP tagged neutral D mesons can be produced in the decay of the $\psi(3770)$ resonance, and these can be used to obtain information about the complex phase of the amplitude f , which is precisely the information required for a model-independent measurement of ϕ_3 .

The method used here has two possible two-fold ambiguities in the determination of the pair of parameters (ϕ_3, δ) . The first one is a shift $(\phi_3, \delta) \rightarrow (\phi_3 + \pi, \delta + \pi)$. The measured phases $\theta_+ = \delta + \phi_3$ and $\theta_- = \delta - \phi_3$ do not change under this transformation. Another ambiguity is the inversion of sign $(\phi_3, \delta) \rightarrow (-\phi_3, -\delta)$ with the simultaneous complex conjugation of the \bar{D}^0 decay amplitude f . This transformation does not change the observables, which are the squared absolute values of the amplitudes. However, if the \bar{D}^0 decay amplitude is approximated by a set of two-body amplitudes, the Breit-Wigner dependence fixes the sign of the imaginary part of the \bar{D}^0 decay amplitude (the complex conjugate Breit-Wigner amplitude does not satisfy the causality requirement), and the second ambiguity is thus resolved.

In a preliminary version of this analysis [7], we used only the $B^\pm \rightarrow \tilde{D} K^\pm$ mode to constrain ϕ_3 . The current measurement is based on two modes, $B^\pm \rightarrow \tilde{D} K^\pm$ and $B^\pm \rightarrow \tilde{D}^* K^\pm (D^* \rightarrow D\pi^0)$. The statistical error evaluation is also improved compared to the previous measurement.

EVENT SELECTION

We use a 140 fb^{-1} data sample collected by the Belle detector. The decays $B^\pm \rightarrow DK^\pm$ and $B^\pm \rightarrow D^* K^\pm$, $D^* \rightarrow D\pi^0$ are selected for the determination of ϕ_3 ; the decays $B^\pm \rightarrow D\pi^\pm$, $B^\pm \rightarrow D^* \pi^\pm$ with $D^* \rightarrow D\pi^0$ and $\bar{B}^0(B^0) \rightarrow D^{*\pm} \pi^\mp$ with $D^{*\pm} \rightarrow D\pi^\pm$ serve as control samples. We require the neutral D meson to decay to the $K_S \pi^+ \pi^-$ final state in all cases. We also select decays of $D^{*\pm} \rightarrow D\pi^\pm$ produced via the $e^+e^- \rightarrow c\bar{c}$ continuum process as a high-statistics sample to determine the $\bar{D}^0 \rightarrow K_S \pi^+ \pi^-$ decay amplitude.

The Belle detector is described in detail elsewhere [9]. It is a large-solid-angle magnetic spectrometer consisting of a three-layer silicon vertex detector (SVD), a 50-layer central drift chamber (CDC) for charged particle tracking and specific ionization measurement (dE/dx), an array of aerogel threshold Čerenkov counters (ACC), time-of-flight scintillation counters (TOF), and an array of 8736 CsI(Tl) crystals for electromagnetic calorimetry (ECL) located inside a superconducting solenoid coil that provides a 1.5 T magnetic field. An iron flux return located outside the coil is instrumented to detect K_L mesons and identify muons (KLM).

Separation of kaons and pions is accomplished by combining the responses of the ACC and the TOF with the dE/dx measurement from the CDC to form a likelihood $\mathcal{L}(h)$ where h is a pion or a kaon. Charged particles are identified as pions or kaons using the likelihood ratio $\mathcal{R}_{\text{PID}}(h) = \mathcal{L}(h)/(\mathcal{L}(K) + \mathcal{L}(\pi))$.

Charged tracks are required to satisfy criteria based on the quality of the track fit and the distance from the interaction point in both longitudinal and transverse planes with respect to the beam axis. To reduce the low momentum combinatorial background we require each track to have a transverse momentum greater than $100 \text{ MeV}/c$. For charged kaon identification, we require the track to have $\mathcal{R}_{\text{PID}}(K) > 0.7$.

Photon candidates are required to have ECL energy greater than 30 MeV. Neutral pion candidates are formed from pairs of photons with invariant masses in the range 120 to 150 MeV/c^2 , or less than two standard deviations from the π^0 mass.

Neutral kaons are reconstructed from pairs of oppositely charged tracks without any pion PID requirement. We require the reconstructed vertex distance from the interaction point in the plane transverse to the beam axis to be more than 1 mm and the invariant mass $M_{\pi\pi}$ to satisfy $|M_{\pi\pi} - M_{K_S}| < 10 \text{ MeV}/c^2$, or less than four standard deviations from the nominal K_S mass.

Selection of $D^{*\pm} \rightarrow D\pi^\pm$

To determine the \bar{D}^0 decay model we use $D^{*\pm}$ mesons produced via the $e^+e^- \rightarrow c\bar{c}$ continuum process. The flavor of the neutral D meson is tagged by the charge of the slow pion (which we denote as π_s) in the decay $D^{*\pm} \rightarrow D\pi_s^\pm$.

To select neutral D candidates we require the invariant mass of the $K_S\pi^+\pi^-$ system to be within 9 MeV/ c^2 of the D^0 mass, M_{D^0} . To select events originating from a $D^{*\pm}$ decay we make a requirement on the difference $\Delta M = M_{K_S\pi^+\pi^-} - M_{K_S\pi^+\pi^-}$ of the invariant masses of the $D^{*\pm}$ and the neutral D candidates: $144.6 \text{ MeV}/c^2 < \Delta M < 146.4 \text{ MeV}/c^2$. To suppress combinatorial background from $B\bar{B}$ events, we require the $D^{*\pm}$ to have momentum in the center-of-mass (CM) frame greater than 2.7 GeV/ c .

The distributions of ΔM and $M_{K_S\pi^+\pi^-}$ for these events are shown in Fig. 2. The signal region bounds are indicated with dashed lines. The resolutions of the selection variables are $\sigma(\Delta M) = 0.38 \text{ MeV}/c^2$ and $\sigma(M_{K_S\pi^+\pi^-}) = 5.4 \text{ MeV}/c^2$. The number of events that pass all selection criteria is 104204. To obtain the number of background events in our sample we fit the ΔM distribution. The background is parameterized with the function $b(\Delta M) \sim (1/\Delta M)\sqrt{(\Delta M/m_\pi)^2 - 1}$; the function describing the signal is a combination of two Gaussian peaks with the same mean value. The fit yields 100870 ± 840 signal events and 3210 ± 50 background events corresponding to a background fraction of 3.1%.

Selection of $B^\pm \rightarrow DK^\pm$

The selection of B candidates is based on the CM energy difference $\Delta E = \sum E_i - E_{\text{beam}}$ and the beam-constrained B meson mass $M_{\text{bc}} = \sqrt{E_{\text{beam}}^2 - (\sum p_i)^2}$, where E_{beam} is the CM beam energy, and E_i and p_i are the CM energies and momenta of the B candidate decay products. We select events with $M_{\text{bc}} > 5.2 \text{ GeV}/c^2$ and $|\Delta E| < 0.2 \text{ GeV}$ for the analysis. The requirements for signal candidates are $5.272 \text{ GeV}/c^2 < M_{\text{bc}} < 5.288 \text{ GeV}/c^2$ and $|\Delta E| < 0.022 \text{ GeV}$. In addition, we make a requirement on the invariant mass of the neutral D candidate: $|M_{K_S\pi\pi} - M_{D^0}| < 11 \text{ MeV}/c^2$.

To suppress background from $e^+e^- \rightarrow q\bar{q}$ ($q = u, d, s, c$) continuum events, we require $|\cos \theta_{\text{thr}}| < 0.8$, where θ_{thr} is the angle between the thrust axis of the B candidate daughters and that of the rest of the event. For additional background rejection, we use a Fisher discriminant composed of 11 parameters [10]: the production angle of the B candidate, the angle of the B thrust axis relative to the beam axis and nine parameters representing the momentum flow in the event relative to the B thrust axis in the CM frame. We apply a requirement on the Fisher discriminant that retains 90% of the signal and rejects 40% of the remaining continuum background.

The ΔE and M_{bc} distributions for $B^\pm \rightarrow DK^\pm$ candidates are shown in Fig. 3. The peak in the ΔE distribution at $\Delta E = 50 \text{ MeV}$ is due to $B^\pm \rightarrow D\pi^\pm$ decays, where the pion is misidentified as a kaon. The ratio of the number of events in the peak at $\Delta E = 50 \text{ MeV}$ and in the signal peak is 0.54 ± 0.11 , which is consistent with the ratio of $B^\pm \rightarrow DK^\pm$ and $B^\pm \rightarrow D\pi^\pm$ branching fractions of $0.079 \pm 0.009 \pm 0.006$ [6] and a 5% π/K misidentification probability for our $\mathcal{R}_{\text{PID}}(K)$ requirement. The $B^\pm \rightarrow DK^\pm$ selection efficiency (11%) is determined from a Monte Carlo (MC) simulation. The number of events passing all selection criteria is 146. The background fraction is determined from a binned fit to the ΔE distribution, in which the signal is represented by a Gaussian distribution with mean $\Delta E = 0$, the $B^\pm \rightarrow D\pi^\pm$ component is represented by a Gaussian distribution with mean $\Delta E = 50 \text{ MeV}$ and the remaining background is modeled by a linear function. The contributions in the signal region are found to be 112 ± 12 signal events, 1.1 ± 0.2 $B^\pm \rightarrow D\pi^\pm$ events and 35 ± 3 events in the linear background. The overall background fraction is $25 \pm 4\%$.

Selection of $B^\pm \rightarrow D^*K^\pm$

For the selection of $B^\pm \rightarrow D^*K^\pm$ events, in addition to the requirements described above, we require the mass difference $\Delta M = M_{K_S\pi^+\pi^-\pi^0} - M_{K_S\pi^+\pi^-}$ of neutral D^* and D candidates to satisfy $140 \text{ MeV}/c^2 < \Delta M < 145 \text{ MeV}/c^2$. Figure 4 shows the ΔE , M_{bc} and ΔM distributions for $B^\pm \rightarrow D^*K^\pm$ candidates. The selection efficiency is 6.2%.

The number of events satisfying the selection criteria is 39. The background fraction is determined in the same way as for $B^\pm \rightarrow DK^\pm$ events. The fit of the ΔE distribution yields 34 ± 6 signal events, 4.4 ± 1.1 events corresponding to the linear background and 0.24 ± 0.08 $B^\pm \rightarrow D^*\pi^\pm$ events in the signal region. The background fraction is $12 \pm 4\%$.

DETERMINATION OF $\bar{D}^0 \rightarrow K_S \pi^+ \pi^-$ DECAY MODEL

The amplitude f of the $\bar{D}^0 \rightarrow K_S \pi^+ \pi^-$ decay is represented by a coherent sum of two-body decay amplitudes plus one non-resonant decay amplitude,

$$f(m_+^2, m_-^2) = \sum_{j=1}^N a_j e^{i\alpha_j} \mathcal{A}_j(m_+^2, m_-^2) + b e^{i\beta}, \quad (3)$$

where N is the total number of resonances, $\mathcal{A}_j(m_+^2, m_-^2)$, a_j and α_j are the matrix element, amplitude and phase, respectively, of the j -th resonance, and b and β are the amplitude and phase of the non-resonant component. The total phase and amplitude are arbitrary. To be consistent with a CLEO analysis [11], we have chosen the $\bar{D}^0 \rightarrow K_S \rho$ mode to have unit amplitude and zero relative phase. The description of the matrix elements follows Ref. [12]. The matrix elements for the resonances are parameterized by Breit-Wigner shapes with D meson and intermediate resonance form factors and angular dependences taken into account. If we consider the decay of \bar{D}^0 into a particle C and a resonance r , with spin J , that subsequently decays into particles A and B , the expression for the matrix element is

$$\mathcal{A} = F_D F_r \frac{s_J}{M_r^2 - M_{AB}^2 - iM_r \Gamma_{AB}},$$

where M_r is the mass of the resonance, M_{AB} is the invariant mass of the AB system, F_D and F_r are the form factors of the \bar{D}^0 and the resonance, respectively, Γ_{AB} is the mass dependent width of the resonance, and s_J accounts for the angular momentum of the resonance. The form factors are the Blatt-Weisskopf penetration factors [13]; both depend on the spin J of the intermediate resonance. We use the following expressions for the form factors:

$$F = 1$$

for $J = 0$,

$$F = \sqrt{\frac{1 + R^2 p_r^2}{1 + R^2 p_{AB}^2}}$$

for $J = 1$, and

$$F = \sqrt{\frac{9 + 3R^2 p_r^2 + R^4 p_r^4}{9 + 3R^2 p_{AB}^2 + R^4 p_{AB}^4}}$$

for $J = 2$. Here R is a parameter that describes the radial size of the meson (either \bar{D}^0 or resonance r), p_{AB} is the daughter particle momentum in the meson rest frame and p_r is its value when $M_{AB} = M_r$ (for F_D the daughters are C and the resonance r , for F_r the daughters are A and B). The radial parameters we use are $R = 5 \text{ GeV}^{-1}$ for the \bar{D}^0 and $R = 1.5 \text{ GeV}^{-1}$ for all intermediate resonances. The mass dependent width is given by

$$\Gamma_{AB} = \Gamma_r \left(\frac{p_{AB}}{p_r} \right)^{2J+1} \left(\frac{M_r}{M_{AB}} \right) F_r^2,$$

where Γ_r is the width of the resonance. The angular term s_J depends on the spin of the resonance. The expressions for scalar, vector and tensor states are:

$$s_0 = 1,$$

$$s_1 = M_{AC}^2 - M_{BC}^2 + \frac{(M_D^2 - M_C^2)(M_B^2 - M_A^2)}{M_r^2},$$

$$s_2 = \left(M_{BC}^2 - M_{AC}^2 + \frac{(M_D^2 - M_C^2)(M_B^2 - M_A^2)}{M_r^2} \right)^2 - \frac{1}{3} \left(M_{AB}^2 - 2M_D^2 - 2M_C^2 + \frac{(M_D^2 - M_C^2)^2}{M_r^2} \right) \left(M_{AB}^2 - 2M_A^2 - 2M_B^2 + \frac{(M_A^2 - M_B^2)^2}{M_r^2} \right).$$

For the \bar{D}^0 model we use a set of 15 two-body amplitudes. These include four Cabibbo-allowed amplitudes: $K^*(892)^+\pi^-$, $K_0^*(1430)^+\pi^-$, $K_2^*(1430)^+\pi^-$ and $K^*(1680)^+\pi^-$; doubly Cabibbo-suppressed partners for each of these states; and seven channels with K_S and a $\pi\pi$ resonance: $K_S\rho$, $K_S\omega$, $K_S f_0(980)$, $K_S f_2(1270)$, $K_S f_0(1370)$, $K_S\sigma_1$ and $K_S\sigma_2$. The masses and Breit-Wigner widths of the scalars σ_1 and σ_2 are left unconstrained, while the masses and widths of other resonances are taken to be the same as in the CLEO analysis [11]. In contrast to the CLEO analysis, we have introduced all doubly Cabibbo-suppressed amplitudes for flavor-specific decays (only $K^*(892)^-\pi^+$ was considered by CLEO) and two scalar states σ_1 and σ_2 . The amplitude for σ_1 describes the excess of events near the low $\pi\pi$ invariant mass edge of the phase space. The resonance σ_2 was introduced to describe a structure near 1.1 GeV^2/c^4 in the $m_{\pi\pi}^2$ distribution. This structure could be due to the decay $f_0(980) \rightarrow \eta\eta$ with rescattering of $\eta\eta$ to $\pi^+\pi^-$, which could distort the $f_0(980) \rightarrow \pi^+\pi^-$ amplitude for $m_{\pi\pi}$ near the $\eta\eta$ production threshold.

We use an unbinned maximum likelihood technique to fit the Dalitz plot distribution to the model described by Eq. 3. We minimize the inverse logarithm of the likelihood function in the form

$$-2 \log L = -2 \left[\sum_{i=1}^n \log p(m_{+,i}^2, m_{-,i}^2) - \log \int_D p(m_+^2, m_-^2) dm_+^2 dm_-^2 \right], \quad (4)$$

where i runs over all selected event candidates, and $m_{+,i}^2, m_{-,i}^2$ are measured Dalitz plot variables. The integral in the second term accounts for the overall normalization of the probability density.

The Dalitz plot density is represented by

$$p(m_+^2, m_-^2) = \varepsilon(m_+^2, m_-^2) \int_{-\infty}^{\infty} |M(m_+^2 + \mu^2, m_-^2 + \mu^2)|^2 \exp\left(-\frac{\mu^2}{2\sigma_m^2(m_{\pi\pi}^2)}\right) d\mu^2 + B(m_+^2, m_-^2), \quad (5)$$

where $M(m_+^2, m_-^2) = f(m_+^2, m_-^2)$ is the decay amplitude described by Eq. 3, $\varepsilon(m_+^2, m_-^2)$ is the efficiency, $B(m_+^2, m_-^2)$ is the background density, $\sigma_m(m_{\pi\pi}^2)$ is the resolution of the squared invariant mass $m_{\pi\pi}^2$ of two pions ($m_{\pi\pi}^2 = M_D^2 + M_K^2 + 2M_\pi^2 - m_+^2 - m_-^2$). The free parameters of the minimization are the amplitudes a_j and phases α_j of the resonances (except for the $K_S\rho$ component, for which the parameters are fixed), the amplitude b and phase β of the non-resonant component and the masses and widths of the σ_1 and σ_2 scalars.

The background density for $\bar{D}^0 \rightarrow K_S\pi^+\pi^-$ events is extracted from ΔM sidebands: $\Delta M < 142 \text{ MeV}/c^2$ and $148 \text{ MeV}/c^2 < \Delta M < 150 \text{ MeV}/c^2$. The background density is parameterized by a third-order polynomial in the variables m_+^2 and m_-^2 to describe the purely combinatorial background, plus Dalitz plot densities for D^0 and \bar{D}^0 decays that correspond to events where a correctly reconstructed \bar{D}^0 is combined with a random slow pion. From the fit, we obtain the fractions of the background components: the purely combinatorial background is $43 \pm 3\%$, combinations of D^0 with a pion of the correct charge account for $49 \pm 3\%$, and the remaining $8 \pm 1\%$ is due to D^0 's combined with a pion of the wrong charge. The background fraction is fixed to 3.1% from the fit to the ΔM distribution. As a consistency check, we also perform a fit with the background fraction floated and obtain a value for the background fraction in agreement with the result from the ΔM fit.

Our analysis is not sensitive to the absolute value of the reconstruction efficiency, but variations of the efficiency across the phase space can effect the fit result. The shape of the efficiency over the Dalitz plot is extracted from a MC simulation, where the \bar{D}^0 decays uniformly over the allowed phase space. The parameterization of the efficiency shape is a third-order polynomial in the variables m_+^2 and m_-^2 , and symmetrical under interchange of π^+ and π^- . The efficiency is nearly uniform over the central part of the Dalitz plot, but drops by between 5% and 13% at the edges of phase space. Finite momentum resolution has to be taken into account in the fit function since our model includes a narrow $\omega \rightarrow \pi^+\pi^-$ state. Although both m_+^2 and m_-^2 have finite resolution, we consider only the resolution of the $m_{\pi\pi}^2$ combination, since the other Dalitz plot projections do not contain any narrow structures. The resolution σ_m as a function of $m_{\pi\pi}$ is parameterized by a linear function and is extracted from MC simulation. The average $m_{\pi\pi}^2$ resolution is $4.8 \times 10^{-3} \text{ GeV}^2/c^4$.

The fit results are given in Table I. The parameters of the σ resonances obtained in the fit are: $M_{\sigma_1} = 539 \pm 9 \text{ MeV}/c^2$, $\Gamma_{\sigma_1} = 453 \pm 16 \text{ MeV}/c^2$, $M_{\sigma_2} = 1048 \pm 7 \text{ MeV}/c^2$, and $\Gamma_{\sigma_2} = 109 \pm 11 \text{ MeV}/c^2$. The $\bar{D}^0 \rightarrow K_S\pi^+\pi^-$

Dalitz plot, as well as its projections with the fit results superimposed, are shown in Fig. 5. The large peak in the m_+^2 distribution corresponds to the dominant $\bar{D}^0 \rightarrow K^*(892)^+\pi^-$ mode. The minimum in the m_-^2 distribution at $0.8 \text{ GeV}^2/c^4$ is due to destructive interference with the doubly Cabibbo suppressed $\bar{D}^0 \rightarrow K^*(892)^-\pi^+$ amplitude. In the $m_{\pi\pi}^2$ distribution, the $\bar{D}^0 \rightarrow K_S\rho$ contribution is visible around $0.5 \text{ GeV}^2/c^4$ with a steep edge on the upper side due to interference with $\bar{D}^0 \rightarrow K_S\omega$. The minimum around $0.9 \text{ GeV}^2/c^4$ is due to the decay $\bar{D}^0 \rightarrow K_S f_0(980)$ interfering destructively with other modes.

We obtain a larger amplitude for the non-resonant component compared to the CLEO analysis [11] (the fit fraction corresponding to the non-resonant component in our case is 24%). The non-resonant component is found to be highly correlated with the amplitude for the σ_1 resonance. A fit with the non-resonant amplitude fixed to zero yields a σ_1 amplitude of 0.78 ± 0.05 , while a fit without the σ_1 yields a non-resonant amplitude of 4.66 ± 0.15 . Therefore, we conclude that the large non-resonant fraction in our \bar{D}^0 model is due to a deficiency in our description of the σ_1 state. We include this effect in the model uncertainty by performing additional fits to the $B^\pm \rightarrow D^{(*)}K^\pm$ data with \bar{D}^0 models with the non-resonant or σ_1 amplitudes excluded.

The unbinned likelihood technique does not provide a reliable criterion for the goodness of fit. To check the quality of the fit, we make use of the large number of events in our sample and perform a binned χ^2 test by dividing the Dalitz plot into square regions $0.05 \times 0.05 \text{ GeV}^2/c^4$. The test yields $\chi^2 = 2121$ for 1130 degrees of freedom. More detailed studies are required in order to understand the precise dynamics of $\bar{D}^0 \rightarrow K_S\pi^+\pi^-$ decay. However, for the purpose of measuring ϕ_3 , we take the fit discrepancy into account in the model uncertainty.

DALITZ PLOT ANALYSIS OF $B^\pm \rightarrow DK^\pm$ DECAY

The Dalitz plots for $\bar{D} \rightarrow K_S\pi^+\pi^-$, which contain information about CP violation in B decays, are shown in Figs. 6 and 7 for $B^\pm \rightarrow \bar{D}K^\pm$ and $B^\pm \rightarrow \bar{D}^*K^\pm$, respectively. These distributions are fitted by minimizing the combined logarithmic likelihood function

$$-2 \log L = -2 \log L_- - 2 \log L_+,$$

where $L_- (L_+)$ are the likelihoods of $B^- (B^+)$ data given by Eq. 4. The corresponding Dalitz plot densities $p_\pm(m_+^2, m_-^2)$ are given by Eq. 5 with decay amplitudes M_\pm described by Eq. 1 (B^+ data) and Eq. 2 (B^- data). The \bar{D}^0 decay model f is fixed, and the free parameters of the fit are the amplitude ratio r and phases ϕ_3 and δ .

As in the study of the sample from continuum $D^{*\pm} \rightarrow D\pi^\pm$ decays, the efficiency and the momentum resolution were extracted from the signal MC sample, where the neutral D meson decays according to phase space. The determination of the background contribution is described below.

Backgrounds

Five sources of background are considered in our analysis (see Table II). We determine the fraction and Dalitz plot shape for each component and use the results in the fit to the signal Dalitz plot. The largest contribution comes from two kinds of continuum events: random combination of tracks, and correctly reconstructed neutral D mesons combined with random kaons. These backgrounds are analyzed using an off-resonance data sample collected at an energy 60 MeV below the $\Upsilon(4S)$ resonance in addition to a sample in which we make requirements on $|\cos\theta_{\text{thr}}|$ and the Fisher discriminant that select continuum events and reject $B\bar{B}$ events. The continuum background fraction is $22.1 \pm 3.9\%$ for $B^\pm \rightarrow DK^\pm$ and $9.0 \pm 3.6\%$ for $B^\pm \rightarrow D^*K^\pm$. The Dalitz plot shape of the continuum background is parameterized by a third-order polynomial in the variables m_+^2 and m_-^2 for the combinatorial background component and a sum of D^0 and \bar{D}^0 shapes for real neutral D mesons combined with random kaons.

The background from $B\bar{B}$ events originates either from a $B^\pm \rightarrow D^{(*)}K^\pm$ decay with some of the final state particles replaced by the decay products of the other B meson, or from other charged or neutral B decays (possibly with misidentified or lost particles). We subdivide the $B\bar{B}$ background into four categories:

1. Decays other than $B^\pm \rightarrow D^{(*)}K^\pm$ and $B^\pm \rightarrow D^{(*)}\pi^\pm$, of which the dominant fraction comes from the decay of $D^{(*)}$ from one B meson, with some particles taken from the other B decay, constitute the largest part of the $B\bar{B}$ background. They are investigated with a generic MC sample. For this, we obtain background fractions of $2.2 \pm 0.2\%$ for $B^\pm \rightarrow DK^\pm$ and $2.1 \pm 0.4\%$ for $B^\pm \rightarrow D^*K^\pm$. The parameterization of this background includes a linear function in the variables m_+^2 and m_-^2 and a Gaussian peak in m_-^2 .

2. The process $B^\pm \rightarrow D^{(*)}\pi^\pm$ with a pion misidentified as a kaon is suppressed by the requirement on the K/π identification probability and on the CM energy difference, ΔE . The fraction of this background is obtained by fitting the ΔE distribution; the corresponding Dalitz plot distribution is that of \bar{D}^0 without the opposite flavor admixture. The fractions for this background are $1.0 \pm 0.2\%$ for $B^\pm \rightarrow DK^\pm$ and $0.6 \pm 0.2\%$ for $B^\pm \rightarrow D^*K^\pm$.
3. $B^\pm \rightarrow D^{(*)}K^\pm$ events where one of the neutral D meson decay products is replaced by a random kaon or pion were studied using a MC data set where one of the charged B mesons from the $\Upsilon(4S)$ decays into the $D^{(*)}K$ state. The corresponding background fraction is $0.4 \pm 0.1\%$ for both $B^\pm \rightarrow DK^\pm$ and $B^\pm \rightarrow D^*K^\pm$ modes; the Dalitz plot shape is parameterized by a linear function in the variables m_+^2 and m_-^2 plus a D^0 amplitude.
4. Events in which a correctly reconstructed neutral D is combined with a random charged kaon are of importance, because half of the kaons have the wrong sign: such events will be misinterpreted as decays of D mesons of the opposite flavor, and thus introduce distortion in the most sensitive area of the Dalitz plot. In the MC sample, we find no events of this kind, which allows us to set an upper limit of 0.4% (at 95% CL) on the fraction for this contribution.

Control sample fits

To test the consistency of the fitting procedure, the same fitting procedure was applied to the $B^\pm \rightarrow \tilde{D}^{(*)}\pi^\pm$ and $\bar{B}^0(B^0) \rightarrow D^{*\pm}\pi^\mp$ control samples as to the $B^\pm \rightarrow \tilde{D}^{(*)}K^\pm$ signal. For decays in which only one flavor D meson can contribute, the fit should return values of the amplitude ratio r consistent with zero. In the case of $B^\pm \rightarrow \tilde{D}^{(*)}\pi^\pm$ a small amplitude ratio is expected ($r \sim |V_{ub}V_{cd}^*|/|V_{cb}V_{ud}^*| \sim 0.02$). Deviations from these values can appear if the Dalitz plot distribution is not well described by the fit model.

For the control sample fits, we consider B^+ and B^- data separately, to check for the absence of CP violation. The free parameters of the Dalitz plot fit are r_\pm and θ_\pm , where $\theta_\pm = \delta \pm \phi_3$ (see Eqs. 1, 2).

The fit results for $B^\pm \rightarrow \tilde{D}\pi^\pm$ are $r_+ = 0.056 \pm 0.028$, $\theta_+ = 237^\circ \pm 27^\circ$ for B^+ data and $r_- = 0.068 \pm 0.026$, $\theta_- = 232^\circ \pm 22^\circ$ for B^- data. It should be noted that since the value of r is positive definite, the error of this parameter does not serve as a good measure of the $r = 0$ hypothesis. To demonstrate the deviation of the amplitude ratio r from zero, the real and imaginary parts of the complex amplitude ratio $re^{i\theta}$ are more suitable. Figure 8 (a) shows the complex amplitude ratio constraints for the B^+ and B^- data separately. It can be seen from the plot that both amplitude ratios differ from the expected value by more than two standard deviations. This deviation is treated as a potential systematic effect.

The other control samples, $B^\pm \rightarrow \tilde{D}^*\pi^\pm$ with \tilde{D}^* decaying to $\tilde{D}\pi^0$, and $\bar{B}^0(B^0) \rightarrow D^{*\pm}\pi^\mp$ with $D^{*\pm} \rightarrow D\pi^\pm$, do not show any significant deviation from $r = 0$. The results of the fit to the $B^\pm \rightarrow \tilde{D}^*\pi^\pm$ sample (351 events) are $r_+ = 0.041 \pm 0.069$, $\theta_+ = 163^\circ \pm 100^\circ$, $r_- = 0.057 \pm 0.054$, $\theta_- = 340^\circ \pm 65^\circ$ and are shown in Fig. 8 (b); the results of the fit to the $\bar{B}^0(B^0) \rightarrow D^{*\pm}\pi^\mp$ sample (517 events) are $r_+ = 0.017 \pm 0.070$, $\theta_+ = 278^\circ \pm 133^\circ$, $r_- = 0.026 \pm 0.050$, $\theta_- = 225^\circ \pm 99^\circ$ and are shown in Fig. 8 (c).

RESULTS

The results of the separate B^+ and B^- data fits are shown in Fig. 9. The plots show the constraints on the complex amplitude ratio $re^{i\theta}$ for the $B^\pm \rightarrow \tilde{D}K^\pm$ and $B^\pm \rightarrow \tilde{D}^*K^\pm$ samples. The fit technique is the same as the one used for the control samples. It can be seen that in both signal samples a significant non-zero value of r is observed. A difference between the phases θ_+ and θ_- is also apparent in both the $B^\pm \rightarrow \tilde{D}K^\pm$ and $B^\pm \rightarrow \tilde{D}^*K^\pm$ samples, which indicates a deviation of ϕ_3 from zero.

A combined unbinned maximum likelihood fit to the B^+ and B^- samples with r , ϕ_3 and δ as free parameters yields the following values: $r = 0.31 \pm 0.11$, $\phi_3 = 86^\circ \pm 17^\circ$, $\delta = 168^\circ \pm 17^\circ$ for the $B^\pm \rightarrow \tilde{D}K^\pm$ sample and $r = 0.34 \pm 0.14$, $\phi_3 = 51^\circ \pm 25^\circ$, $\delta = 302^\circ \pm 25^\circ$ for the $B^\pm \rightarrow \tilde{D}^*K^\pm$ sample. The errors quoted here are obtained from the likelihood fit. These errors are a good representation of the uncertainties for a Gaussian likelihood distribution, however in our case the distributions are highly non-Gaussian. In addition, the errors for the strong and weak phases depend on the values of the amplitude ratio r (e.g. for $r = 0$ there is no sensitivity to the phases). A more reliable estimate of the statistical uncertainties is obtained using a large number of MC pseudo-experiments as discussed below.

Estimation of model uncertainty

The model used for the $\bar{D}^0 \rightarrow K_S \pi^+ \pi^-$ decay is one of the main sources of systematic error for our analysis. The model is a result of the fit to an experimental Dalitz plot, however, since the density of the plot is proportional to the absolute value squared of the decay amplitude, the phase $\phi(m_+^2, m_-^2)$ of the complex amplitude is not directly measured. The phase variations across the Dalitz plot are therefore the result of model assumptions and their uncertainties may affect the \tilde{D} Dalitz plot fit from $B^\pm \rightarrow \tilde{D}^{(*)} K^\pm$.

To estimate the effects of the model uncertainties, a MC simulation is used. Event samples are generated according to the Dalitz distribution described by the amplitude given by Eq. 1 with the resonance parameters extracted from our fit of continuum D^0 data, but to fit this simulated plot different models for $f(m_+, m_-)$ are used (see Table III). We scan the phases ϕ_3 and δ in their physical regions and take the maximum deviations of the fit parameters ($(\Delta r)_{\max}$, $(\Delta\phi_3)_{\max}$, and $(\Delta\delta)_{\max}$) as model uncertainty estimates. The values for $(\Delta r)_{\max}$, $(\Delta\phi_3)_{\max}$ and $(\Delta\delta)_{\max}$ quoted in Table III are obtained with the value $r = 0.13$. For larger r values, the model uncertainty tends to be smaller, so our estimate of the model uncertainty is conservative.

All the fit models are based on Breit-Wigner parameterizations of resonances as in our default model. Since a Breit-Wigner amplitude can only describe narrow resonances well, the usual technique to deal with broad states is to introduce Blatt-Weisskopf form factors for the \bar{D}^0 meson (F_D) and intermediate resonance (F_r) and a q^2 -dependence of the resonance width Γ . These quantities have substantial theoretical uncertainties and might introduce a large model error. We have therefore used a fit model without Blatt-Weisskopf form factors and with a constant resonance width to estimate such an error. We have also used a model containing only narrow resonances ($K^*(892)$, ρ , doubly Cabibbo-suppressed $K^*(892)$ and $f^0(980)$) with the wide ones approximated by the flat non-resonant term. The study of the model errors is summarized in Table III. Our estimate of the systematic uncertainty on ϕ_3 is 11° .

Estimation of systematic errors

In addition to the model uncertainty, there are other potential sources of systematic error, such as uncertainties in the background Dalitz plot density, efficiency variations over the phase space and possible fit biases. These are listed in Table IV for the $B^\pm \rightarrow \tilde{D} K^\pm$ and $B^\pm \rightarrow \tilde{D}^* K^\pm$ modes separately. The component related to the background shape parameterization was estimated by extracting the background shape from the M_D sidebands and by using a flat background distribution. The maximum deviation of the fit parameters from the ‘‘standard’’ background parameterization was assigned as the corresponding systematic error. The effect of the uncertainty in the background fraction was studied by varying the background fraction by one standard deviation.

A potentially dangerous background is caused by events with a random kaon, half of which would not have the correct charge. We set a 0.4% upper limit on this kind of background at 95% confidence level based on MC simulation. The effect of this background on the fit results was studied using a MC procedure similar to that used for investigating the model uncertainty. The bias in the fit parameters corresponding to a 0.4% fraction is negligible (0.7° for ϕ_3) in comparison to the systematic error due to background shape.

As mentioned above, the efficiency shape and momentum resolution were extracted from MC simulation. To estimate their contributions to the systematic error, we repeat the fit using a flat efficiency and a fit model that does not take the resolution into account, respectively. The biases due to the efficiency shape differ for $B^\pm \rightarrow \tilde{D} K^\pm$ and $B^\pm \rightarrow \tilde{D}^* K^\pm$ samples, but since we expect the values of the efficiency systematics to be close for the two modes, we assign the maximum value of the bias as the corresponding systematic error.

The non-zero amplitude ratio observed in the $B^\pm \rightarrow \tilde{D} \pi^\pm$ control sample can be either due to a statistical fluctuation or may indicate some systematic effect such as background structure or a deficiency of the \bar{D}^0 decay model. Since the source of this bias is unknown, we conservatively treat it as an additional systematic effect. The corresponding bias of parameters is estimated in the following way. Suppose the parameters in the $re^{i\theta}$ plane are biased by a value Δr in a certain direction, then the maximum bias of the total phases would be equal to $(\Delta\theta)_{\max} \sim \Delta r/r \sim 11^\circ$. Since $\delta = (\theta_+ + \theta_-)/2$ and $\phi_3 = (\theta_+ - \theta_-)/2$, the maximum biases of the strong and weak phases would also be equal to 11° . The maximum bias of r for the simultaneous fit to both flavors in the case of $\phi_3 \sim \pi$ would be $\Delta r = \sqrt{r^2 + (\Delta r)^2} - r \sim 0.006$.

Evaluation of statistical error

We use a frequentist technique to evaluate the statistical significance of the measurements. This method requires knowledge of the probability density function (PDF) of the fitted parameters as a function of the true parameters.

To obtain this PDF, we employ a “toy” MC technique that uses a simplified MC simulation of the experiment which incorporates the same efficiencies, resolution and backgrounds as used in the fit to the experimental data. This MC is used to generate several hundred experiments for a given set of r , θ_+ and θ_- values. For each simulated experiment, Dalitz plot distributions are generated with numbers of events that nearly equal to the numbers of events observed in the data — 70 events for each B flavor for $B^\pm \rightarrow \tilde{D}K^\pm$ and 20 events for each B flavor for $B^\pm \rightarrow \tilde{D}^*K^\pm$ — and the simulated Dalitz distributions are subjected to the same fitting procedure that is applied to the data. This is repeated for different values of r , producing distributions of the fitted parameters that are used to produce a functional form of the PDFs for reconstructed values for any set of input parameters.

We parameterize the PDF of a set of fitted parameters (r, ϕ_3, δ) , using the following model. We assume that as a result of the fit of a single Dalitz plot (either B^+ or B^- data), the errors of parameters $Re(r_\pm e^{i\theta_\pm})$ and $Im(r_\pm e^{i\theta_\pm})$ are uncorrelated and have Gaussian distributions with equal RMS which we denote as σ . The PDF of the parameters (r_\pm, θ_\pm) for the true parameters $(\bar{r}_\pm, \bar{\theta}_\pm)$ is thus written as

$$d^2 P(r_\pm, \theta_\pm | \bar{r}_\pm, \bar{\theta}_\pm) = \frac{1}{2\pi\sigma^2} \exp \left[-\frac{(r_\pm \cos \theta_\pm - \bar{r} \cos \bar{\theta}_\pm)^2 + (r_\pm \sin \theta_\pm - \bar{r} \sin \bar{\theta}_\pm)^2}{2\sigma^2} \right] r_\pm dr_\pm d\theta_\pm.$$

To obtain the PDF for the parameters (r, ϕ_3, δ) we fix $r = r_+ = r_-$ and substitute the total phases with $\delta + \phi_3$ and $\delta - \phi_3$:

$$\frac{d^3 P}{dr d\phi_3 d\delta}(r, \phi_3, \delta | \bar{r}, \bar{\phi}_3, \bar{\delta}) = \frac{d^2 P}{dr_+ d\theta_+}(r, \delta + \phi_3 | \bar{r}, \bar{\delta} + \bar{\phi}_3) \frac{d^2 P}{dr_- d\theta_-}(r, \delta - \phi_3 | \bar{r}, \bar{\delta} - \bar{\phi}_3). \quad (6)$$

In this model, there is only one free parameter σ which is obtained from the unbinned maximum likelihood fit of the MC distribution of fitted parameters to Eq. 6. The values of σ obtained for MC samples with different values of r are all equal within 4%, therefore we use a constant value $\sigma = 0.14$ for the PDF of $B^\pm \rightarrow \tilde{D}K^\pm$ data. For the fit of the sample of neutral D mesons from $B^\pm \rightarrow \tilde{D}^*K^\pm$ the value of σ is equal to 0.22.

After the PDF of the fitted parameters is obtained, the confidence level α for each set of true parameters $(\bar{r}, \bar{\phi}_3, \bar{\delta})$ is defined as

$$\alpha(\bar{r}, \bar{\phi}_3, \bar{\delta}) = \int_{\Omega} \frac{d^3 P}{dr d\phi_3 d\delta}(r, \phi_3, \delta | \bar{r}, \bar{\phi}_3, \bar{\delta}) dr d\phi_3 d\delta,$$

where the corresponding confidence region Ω is given by the condition

$$\frac{d^3 P}{dr d\phi_3 d\delta}(r, \phi_3, \delta | \bar{r}, \bar{\phi}_3, \bar{\delta}) \geq \frac{d^3 P}{dr d\phi_3 d\delta}(0.31, 86^\circ, 168^\circ | \bar{r}, \bar{\phi}_3, \bar{\delta}),$$

i.e. it includes all points in the fit parameter space for which the PDF is larger than that at the point $0.31, 86^\circ, 168^\circ$, corresponding to the fit result. For $B^\pm \rightarrow \tilde{D}^*K^\pm$ these values are replaced by $0.34, 51^\circ$ and 302° for r, ϕ_3 and δ , respectively.

The confidence regions for the pairs of parameters (ϕ_3, δ) and (ϕ_3, r) are shown in Fig. 10 ($B^\pm \rightarrow \tilde{D}K^\pm$ mode) and Fig. 11 ($B^\pm \rightarrow \tilde{D}^*K^\pm$ mode). These plots are the projections of the corresponding confidence regions in the three-dimensional parameter space. We show the 20%, 74% and 97% confidence level regions, which correspond to one, two, and three standard deviations for a three-dimensional Gaussian distribution. The 20% confidence region, which corresponds to one standard deviation, yields the following results for the fit parameters: $r = 0.26_{-0.14}^{+0.10}$, $\phi_3 = 86^\circ \pm 23^\circ$, $\delta = 168^\circ \pm 23^\circ$ for $B^\pm \rightarrow \tilde{D}K^\pm$ data and $r = 0.20_{-0.17}^{+0.19}$, $\phi_3 = 51^\circ \pm 46^\circ$, $\delta = 302^\circ \pm 46^\circ$ for $B^\pm \rightarrow \tilde{D}^*K^\pm$ data. The central values presented are obtained by maximizing the fit parameters' PDF. This technique accounts for the parameter biases introduced by the fit procedure. We find that ϕ_3 and δ are unbiased in both the $B^\pm \rightarrow DK^\pm$ and $B^\pm \rightarrow D^*K^\pm$ cases, while the central value of r is biased by the fit procedure due to its positive definiteness.

The values of the amplitude ratio r obtained are larger than our initial estimate ($r = 0.13$), though they agree within the statistical error. These values are also consistent with the recent measurement by BABAR collaboration [15], which set up an upper limit $r < 0.22$ at 90% CL for the $B^\pm \rightarrow DK^\pm$ mode.

In the frequentist approach, the significance of the CP violation is evaluated by finding the confidence level for the most probable CP conserving point, *i.e.* the point with $r = 0$ or $\phi_3 = 0$, for which the confidence level $\alpha(\bar{r}, \bar{\phi}_3, \bar{\delta})$ is

minimal. This procedure gives $\alpha = 97\%$ for the point $r = 0.03$, $\phi_3 = 0$, $\delta = 168^\circ$ for the $B^\pm \rightarrow \tilde{D}K^\pm$ sample. The same procedure applied to $B^\pm \rightarrow \tilde{D}^*K^\pm$ sample gives a CP violation significance of 23% (for the point $r = 0.10$, $\phi_3 = 0$, $\delta = 302^\circ$).

Combined ϕ_3 measurement using $B^\pm \rightarrow DK^\pm$ and $B^\pm \rightarrow D^*K^\pm$ samples

The two events samples, $B^\pm \rightarrow DK^\pm$ and $B^\pm \rightarrow D^*K^\pm$, are combined in order to obtain a more accurate measurement of ϕ_3 . The technique we use to obtain the combined measurement is also based on a frequentist approach. Since in general the values of the amplitude ratio r and strong phase δ can differ for the two modes, we have five true parameters ($\bar{\phi}_3, \bar{r}_1, \bar{r}_2, \bar{\delta}_1$ and $\bar{\delta}_2$, where the indices 1 and 2 correspond to $B^\pm \rightarrow DK^\pm$ and $B^\pm \rightarrow D^*K^\pm$ modes, respectively) and six reconstructed parameters (r, ϕ_3 and δ for each of the two modes). Since in this case the physical range of the parameters is smaller than the range of the reconstructed parameters (ϕ_3 values have to be equal for the two modes), the Feldman-Cousins [14] approach is used.

The PDF for the reconstructed parameters is written as

$$\frac{dP}{dx}(x, \mu) = \frac{d^3 P_{B \rightarrow D^0 K}}{dr d\phi_3 d\delta}(r_1, (\phi_3)_1, \delta_1 | \bar{r}_1, \bar{\phi}_3, \bar{\delta}_1) \frac{d^3 P_{B \rightarrow D^* 0 K}}{dr d\phi_3 d\delta}(r_2, (\phi_3)_2, \delta_2 | \bar{r}_2, \bar{\phi}_3, \bar{\delta}_2),$$

where $x = (dr_1, d(\phi_3)_1, d\delta_1, dr_2, d(\phi_3)_2, d\delta_2)$ is a vector of the reconstructed parameters, and $\mu = (\bar{\phi}_3, \bar{r}_1, \bar{r}_2, \bar{\delta}_1, \bar{\delta}_2)$ is a vector of the true parameters.

The confidence level α for a vector of true parameters μ is defined as

$$\alpha(\mu) = \int_{\Omega} \frac{dP}{dx}(x|\mu) dx.$$

The confidence region Ω is given by the Feldman-Cousins likelihood ratio ordering:

$$\frac{dP}{dx}(x, \mu) \bigg/ \frac{dP}{dx}(x, \mu_{best}(x)) > \frac{dP}{dx}(x_0, \mu) \bigg/ \frac{dP}{dx}(x_0, \mu_{best}(x_0)).$$

Here $\mu_{best}(x)$ is defined as the vector of true parameters that maximizes the PDF for a given set x of reconstructed parameters.

The vector of the central values of the true parameters is given by $\alpha = 0$ and equals $\mu_{best}(x_0)$. The corresponding central value of ϕ_3 is 77° . The one standard deviation interval for ϕ_3 (which corresponds to the 3.7% confidence level for the case of a five-dimensional Gaussian distribution) is $\phi_3 = 77^\circ \text{ }^{+17^\circ}_{-19^\circ}$; the two standard deviation (or 45% CL for a five-dimensional distribution) interval is $39^\circ < \phi_3 < 112^\circ$. These intervals include only the statistical error. The statistical significance of CP violation for the combined measurement is 95%.

Since the $B^\pm \rightarrow DK^\pm$ contribution dominates in the combined measurement, we use its value of the systematic uncertainty, which is 13° , as an estimate of the systematic uncertainty in the combined ϕ_3 measurement. The model uncertainty for the two modes is the same and amounts to 11° . The two standard deviation interval including the systematic and model uncertainties is $26^\circ < \phi_3 < 126^\circ$.

CONCLUSION

We report results of a measurement of the unitarity triangle angle ϕ_3 that uses a new method based on a Dalitz plot analysis of the three-body D^0 decay in the process $B^\pm \rightarrow D^{(*)}K^\pm$. The first measurement of ϕ_3 using this technique was performed based on 140 fb^{-1} data sample collected by the Belle detector. From the combination of $B^\pm \rightarrow DK^\pm$ and $B^\pm \rightarrow D^*K^\pm$ modes, we obtain the value of $\phi_3 = 77^\circ \text{ }^{+17^\circ}_{-19^\circ} \pm 13^\circ \pm 11^\circ$. The first error is statistical, the second is experimental systematics and the third is model uncertainty. The two standard deviation interval (including model and systematic uncertainties) is $26^\circ < \phi_3 < 126^\circ$. The statistical significance of CP violation for the combined measurement is 95%. The method allows us to obtain a value of the D^0 - \bar{D}^0 amplitude ratio r , which can be used in other ϕ_3 measurements. We obtain $r = 0.26 \text{ }^{+0.10}_{-0.14} \pm 0.03 \pm 0.04$ for the $B^\pm \rightarrow DK^\pm$ mode and $r = 0.20 \text{ }^{+0.19}_{-0.17} \pm 0.02 \pm 0.04$ for the $B^\pm \rightarrow D^*K^\pm$ mode.

The method has a number of advantages over the other ways to measure ϕ_3 [3]. It is directly sensitive to the value of ϕ_3 and has only the two-fold discrete ambiguity ($\phi_3 + \pi, \delta + \pi$). It does not involve branching fraction measurements and, therefore, the influence of the detector systematics is minimal. The statistical sensitivity of this technique is also superior in the presence of background since an interference term is measured.

Acknowledgments

We are grateful to V. Chernyak and M. Gronau for fruitful discussions. We thank the KEKB group for the excellent operation of the accelerator, the KEK Cryogenics group for the efficient operation of the solenoid, and the KEK computer group and the National Institute of Informatics for valuable computing and Super-SINET network support. We acknowledge support from the Ministry of Education, Culture, Sports, Science, and Technology of Japan and the Japan Society for the Promotion of Science; the Australian Research Council and the Australian Department of Education, Science and Training; the National Science Foundation of China under contract No. 10175071; the Department of Science and Technology of India; the BK21 program of the Ministry of Education of Korea and the CHEP SRC program of the Korea Science and Engineering Foundation; the Polish State Committee for Scientific Research under contract No. 2P03B 01324; the Ministry of Science and Technology of the Russian Federation; the Ministry of Education, Science and Sport of the Republic of Slovenia; the National Science Council and the Ministry of Education of Taiwan; and the U.S. Department of Energy.

* on leave from Fermi National Accelerator Laboratory, Batavia, Illinois 60510

† on leave from Nova Gorica Polytechnic, Nova Gorica

- [1] M. Kobayashi and T. Maskawa, *Prog. Theor. Phys.* **49**, 652 (1973); N. Cabibbo, *Phys. Rev. Lett.* **10**, 531 (1963);
- [2] I. I. Bigi and A. I. Sanda, *Phys. Lett.* **B211**, 213 (1988).
- [3] M. Gronau and D. Wyler, *Phys. Lett.* **B265**, 172 (1991); I. Dunietz, *Phys. Lett.* **B270**, 75 (1991); D. Atwood, G. Eilam, M. Gronau and A. Soni, *Phys. Lett.* **B341**, 372 (1995); D. Atwood, I. Dunietz and A. Soni, *Phys. Rev. Lett.* **78**, 3257 (1997).
- [4] A. Giri, Yu. Grossman, A. Soffer, J. Zupan, *Phys. Rev. D* **68**, 054018(2003).
This technique was proposed independently in the Belle Collaboration, and the analysis of experimental data was under way before the A. Giri *et al.* publication appeared (Proceedings of BINP Special Analysis Meeting on Dalitz Analysis, 24-26 Sep. 2002, unpublished).
- [5] Belle Collaboration, P. Krokovny *et al.*, *Phys. Rev. Lett.* **90**, 141802 (2003).
- [6] Belle Collaboration, K. Abe *et al.*, *Phys. Rev. Lett.* **87**, 111801 (2001).
- [7] Belle Collaboration, K. Abe *et al.*, hep-ex/0308043.
- [8] M. Gronau, *Phys. Lett. B* **557**, 198 (2003).
- [9] Belle Collaboration, A. Abashian *et al.*, *Nucl. Instr. and Meth. A* **479**, 117 (2002).
- [10] CLEO Collaboration, D. M. Asner *et al.*, *Phys. Rev. D* **53**, 1039 (1996).
- [11] CLEO Collaboration, H. Muramatsu *et al.*, *Phys. Rev. Lett.* **89**, 251802 (2002), Erratum-ibid: **90**, 059901 (2003).
- [12] CLEO Collaboration, S. Kopp *et al.*, *Phys. Rev. D* **63**, 092001 (2001).
- [13] J. Blatt and V. Weisskopf, *Theoretical Nuclear Physics*. New York: John Wiley & Sons (1952).
- [14] G. J. Feldman and R. D. Cousins, *Phys. Rev. D* **57**, 3873 (1998).
- [15] BABAR Collaboration, B. Aubert *et al.*, hep-ex/0402024.

TABLE I: Fit results for $\bar{D}^0 \rightarrow K_S \pi^+ \pi^-$ decay. Errors are statistical only. The results for the σ_1, σ_2 masses and widths are given in the text.

Intermediate state	Amplitude	Phase ($^\circ$)
$K^*(892)^+ \pi^-$	1.656 ± 0.012	137.6 ± 0.6
$K^*(892)^- \pi^+$	$(14.9 \pm 0.7) \times 10^{-2}$	325.2 ± 2.2
$K_0^*(1430)^+ \pi^-$	1.96 ± 0.04	357.3 ± 1.5
$K_0^*(1430)^- \pi^+$	0.30 ± 0.05	128 ± 8
$K_2^*(1430)^+ \pi^-$	1.32 ± 0.03	313.5 ± 1.8
$K_2^*(1430)^- \pi^+$	0.21 ± 0.03	281 ± 9
$K^*(1680)^+ \pi^-$	2.56 ± 0.22	70 ± 6
$K^*(1680)^- \pi^+$	1.02 ± 0.2	103 ± 11
$K_S \rho^0$	1.0 (fixed)	0 (fixed)
$K_S \omega$	$(33.0 \pm 1.3) \times 10^{-3}$	114.3 ± 2.3
$K_S f_0(980)$	0.405 ± 0.008	212.9 ± 2.3
$K_S f_0(1370)$	0.82 ± 0.10	308 ± 8
$K_S f_2(1270)$	1.35 ± 0.06	352 ± 3
$K_S \sigma_1$	1.66 ± 0.11	218 ± 4
$K_S \sigma_2$	0.31 ± 0.05	236 ± 11
non-resonant	6.1 ± 0.3	146 ± 3

TABLE II: Fractions of different background sources.

Background source	$B^\pm \rightarrow DK^\pm$	$B^\pm \rightarrow D^* K^\pm$
$q\bar{q}$ combinatorial	$22.1 \pm 3.9\%$	$9.0 \pm 3.6\%$
$B\bar{B}$ events other than $B^\pm \rightarrow D^{(*)} K^\pm / \pi^\pm$	$2.2 \pm 0.2\%$	$2.1 \pm 0.4\%$
$B^\pm \rightarrow D^{(*)} \pi^\pm$ with K/π misID	$1.0 \pm 0.2\%$	$0.6 \pm 0.2\%$
Combinatorics in D^0 decay	$0.4 \pm 0.1\%$	$0.4 \pm 0.1\%$
Combinatorial kaon in $B^\pm \rightarrow D^{(*)} K^\pm$ decay	$<0.4\%$ (95% CL)	$<0.4\%$ (95% CL)
Total	$25 \pm 4\%$	$12 \pm 4\%$

TABLE IV: Contributions to the experimental systematic error.

Source	$B^\pm \rightarrow \tilde{D} K^\pm$			$B^\pm \rightarrow \tilde{D}^* K^\pm$		
	Δr	$\Delta\phi_3$ ($^\circ$)	$\Delta\delta$ ($^\circ$)	Δr	$\Delta\phi_3$ ($^\circ$)	$\Delta\delta$ ($^\circ$)
Background shape	0.017	4.7	2.3	0.016	1.5	2.6
Background fraction	0.025	0.1	0.6	0.015	0.6	0.9
Efficiency shape	0.004	3.5	1.2	0.002	3.5	1.2
Momentum resolution	0.010	2.5	0.6	0.010	2.5	0.6
Control sample bias	0.006	11	11	0.006	11	11
Total	0.032	13	11	0.024	12	11

TABLE III: Estimation of model uncertainty.

Fit model	$(\Delta r)_{\max}$	$(\Delta\phi_3)_{\max}$ ($^\circ$)	$(\Delta\delta)_{\max}$ ($^\circ$)
$F_r = F_D = 1$	0.01	3.1	3.3
$\Gamma(q^2) = \text{Const}$	0.02	4.7	9.0
Narrow resonances plus non-resonant term	0.03	9.9	18.2
Total	0.04	11	21

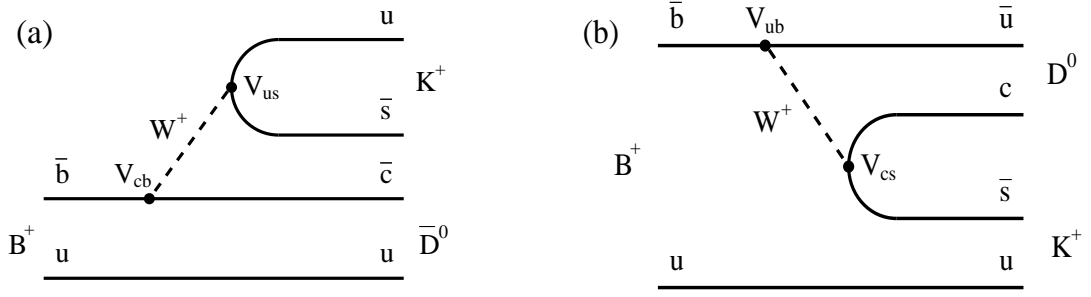


FIG. 1: Feynman diagrams of (a) dominant $B^+ \rightarrow \bar{D}^0 K^+$ and (b) suppressed $B^+ \rightarrow D^0 K^+$ decays

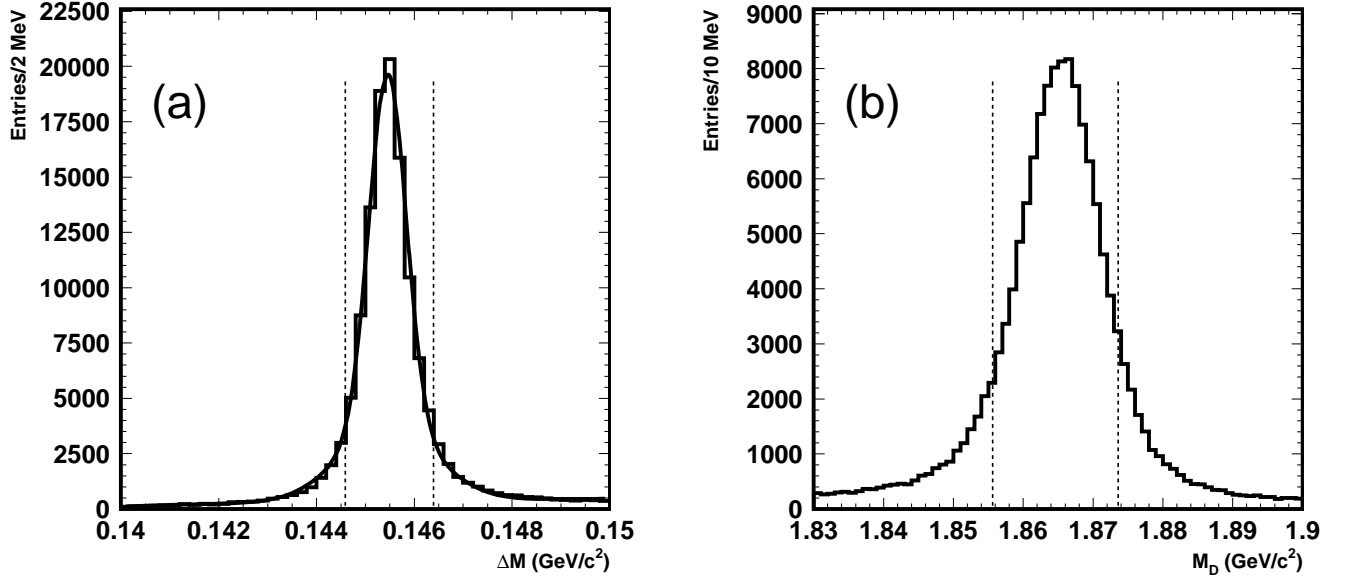


FIG. 2: (a) ΔM and (b) M_D distributions for the $D^{*\pm} \rightarrow D\pi_s^\pm$ candidates. Dashed lines show the signal region. The histogram shows the data; the smooth curve in (a) is the fit result.

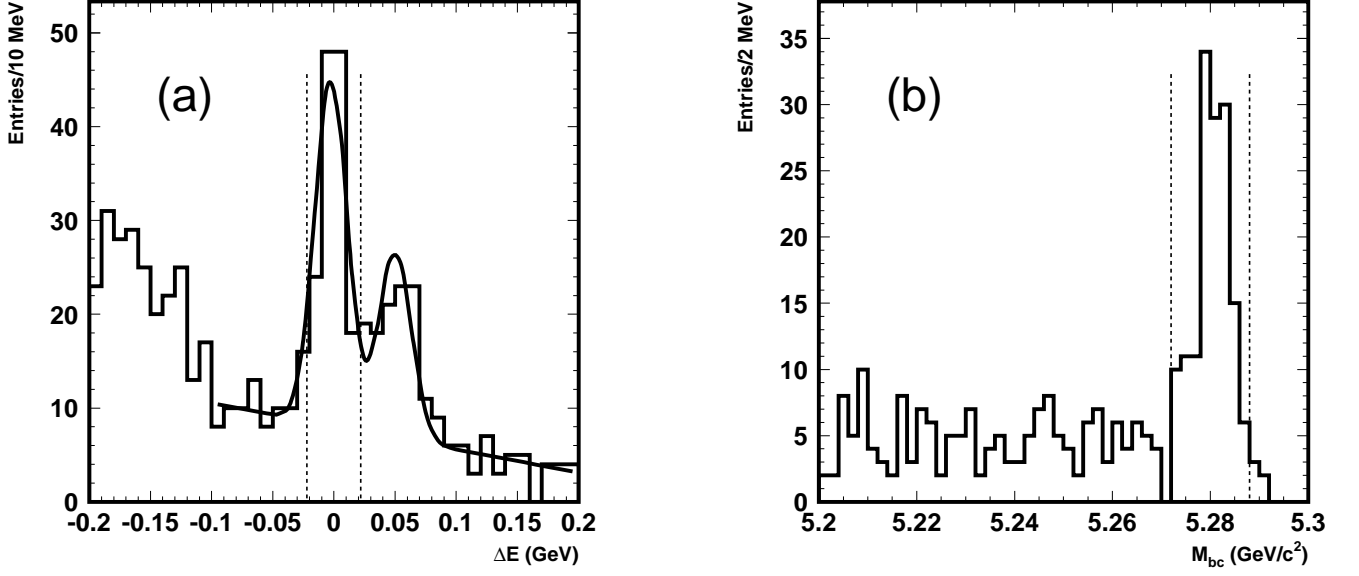


FIG. 3: (a) ΔE and (b) M_{bc} distributions for the $B^\pm \rightarrow DK^\pm$ candidates. Dashed lines show the signal region. The histogram shows the data; the smooth curve in (a) is the fit result.

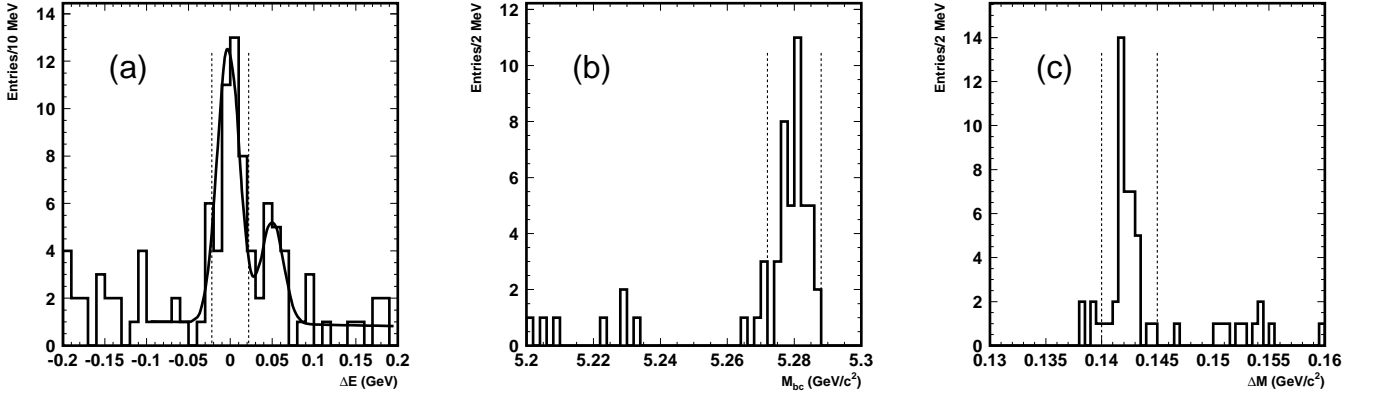


FIG. 4: (a) ΔE , (b) M_{bc} and (c) ΔM distributions for the $B^\pm \rightarrow D^*K^\pm$ candidates. Dashed lines show the signal region. The histogram shows the data; the smooth curve in (a) is the fit result.

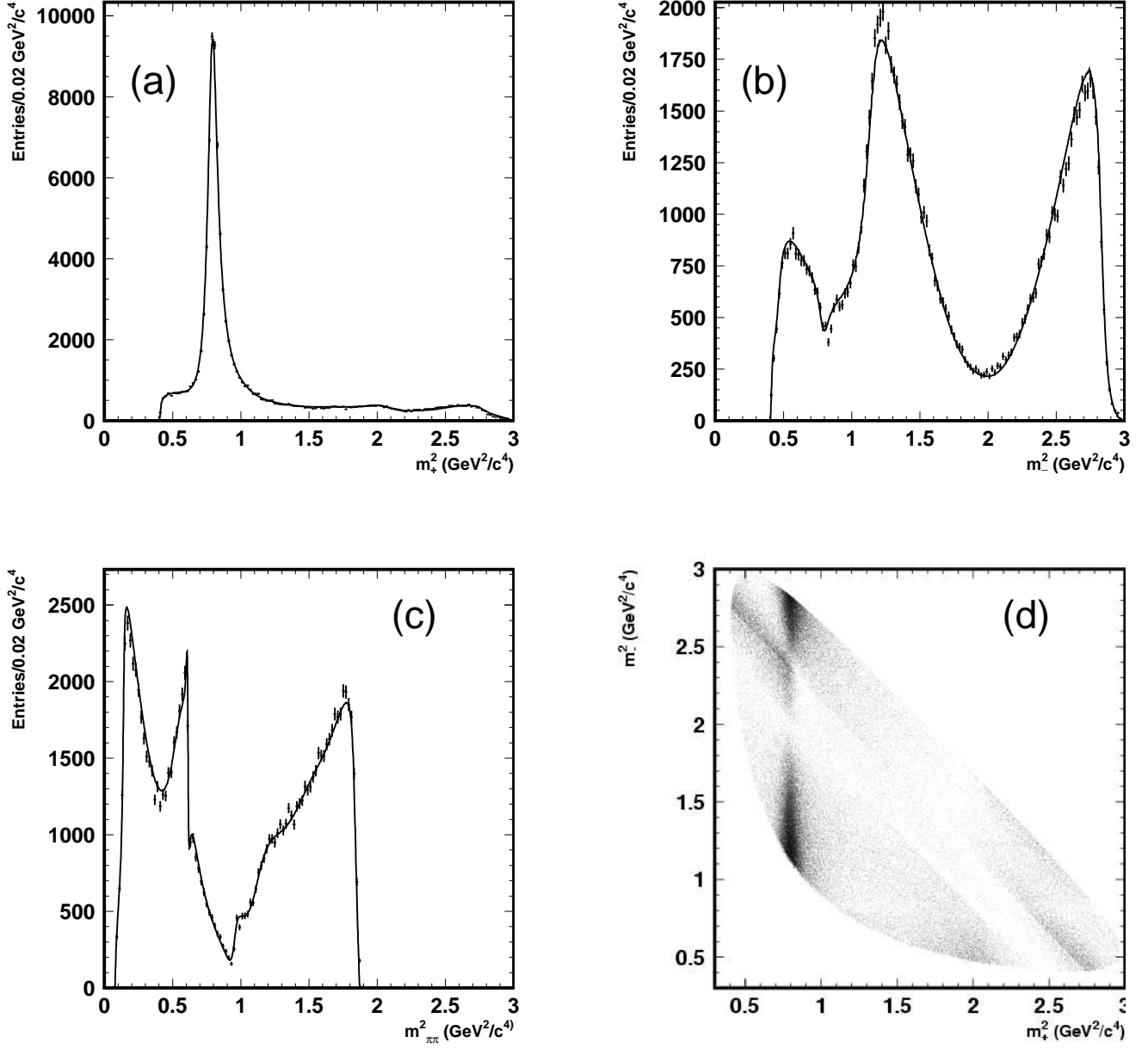


FIG. 5: (a) m_+^2 , (b) m_-^2 , (c) $m_{\pi\pi}^2$ distributions and (d) Dalitz plot for the $\bar{D}^0 \rightarrow K_S \pi^+ \pi^-$ decay from the $D^{*\pm} \rightarrow D \pi_s^\pm$ process. The points with error bars show the data, the smooth curve is the fit result.

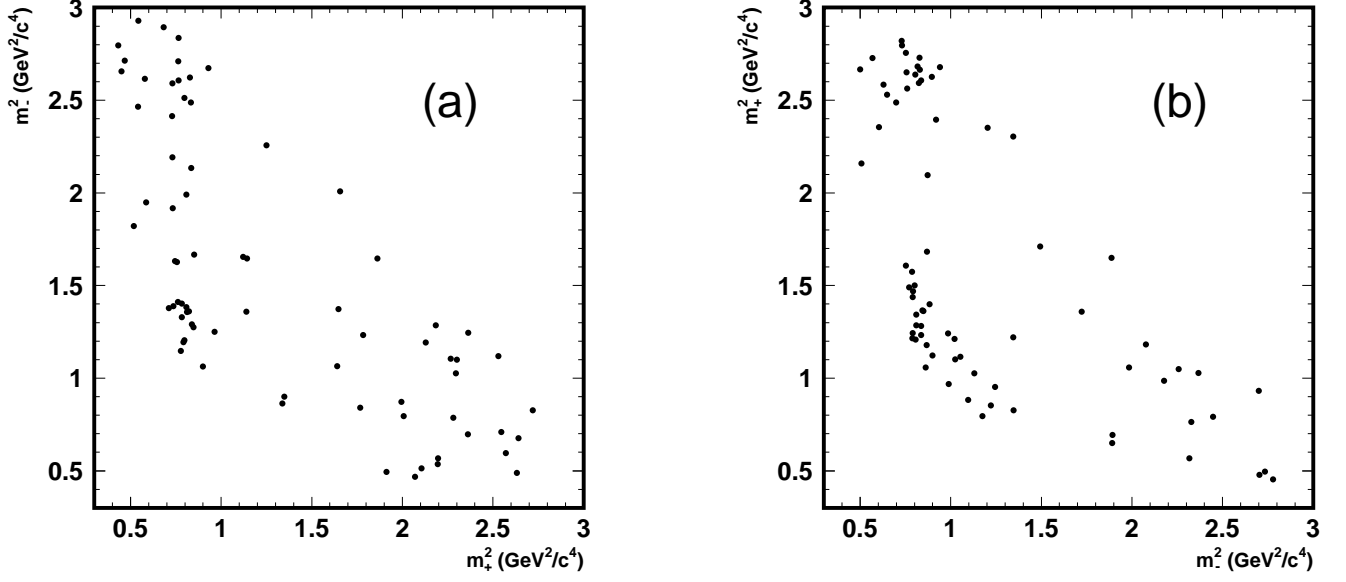


FIG. 6: Dalitz plots of $\tilde{D} \rightarrow K_S \pi^+ \pi^-$ decay from (a) $B^+ \rightarrow \tilde{D} K^+$ and (b) $B^- \rightarrow \tilde{D} K^-$.

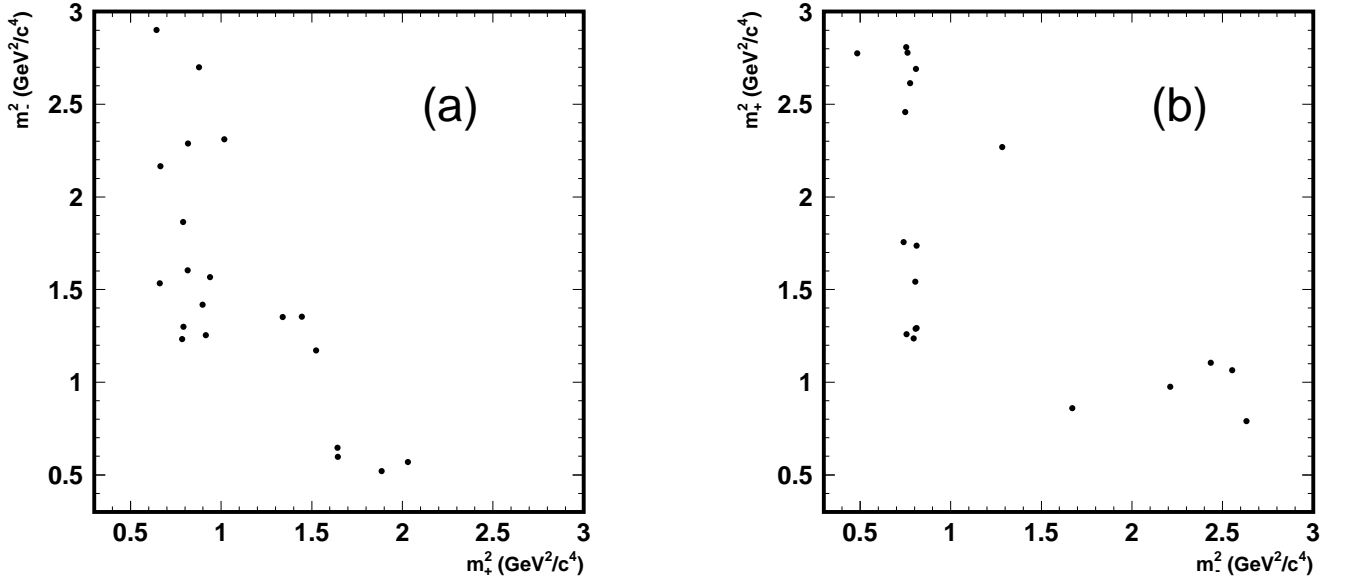


FIG. 7: Dalitz plots of $\tilde{D} \rightarrow K_S \pi^+ \pi^-$ decay from (a) $B^+ \rightarrow \tilde{D}^* K^+$ and (b) $B^- \rightarrow \tilde{D}^* K^-$.

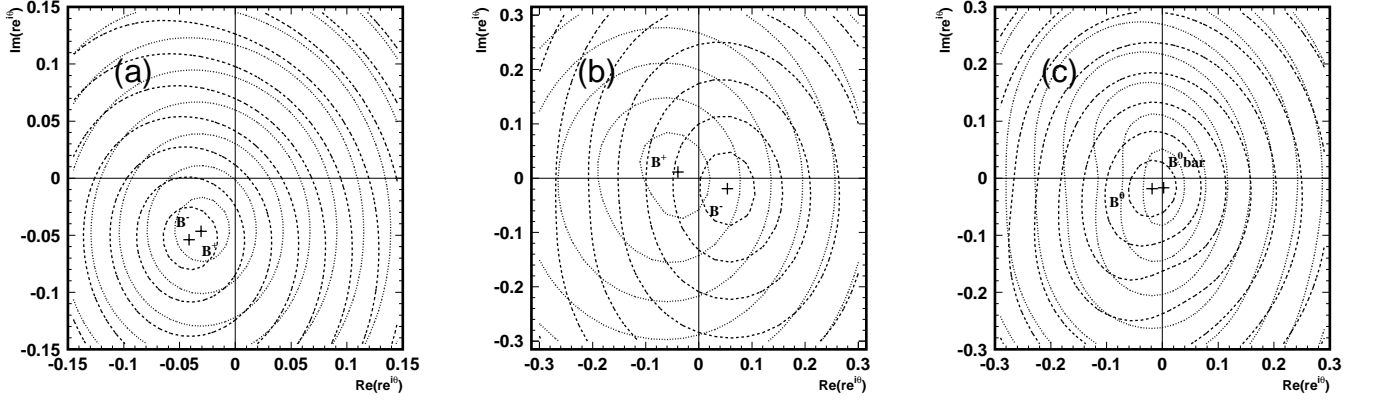


FIG. 8: Constraint plots of the complex amplitude ratio $re^{i\theta}$ for (a) $B^\pm \rightarrow \tilde{D}\pi^\pm$, (b) $B^\pm \rightarrow \tilde{D}^*\pi^\pm$ and (c) $\bar{B}^0(B^0) \rightarrow D^{*\pm}\pi^\mp$ decays. Contours indicate integer multiples of the standard deviation. Dotted contours are from B^+ (\bar{B}^0) data, dashed contours are from B^- (B^0) data.

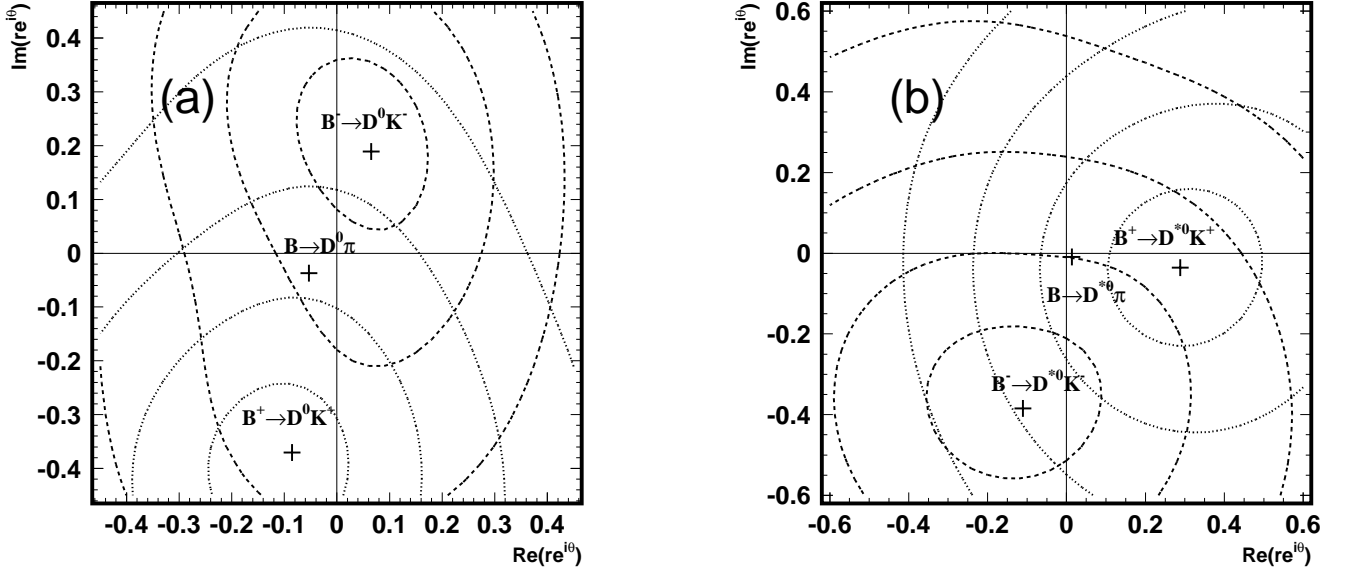


FIG. 9: Constraint plots of the complex amplitude ratio $re^{i\theta}$ for (a) $B^\pm \rightarrow \tilde{D}K^\pm$ and (b) $B^\pm \rightarrow \tilde{D}^*K^\pm$ decays. Contours indicate integer multiples of the standard deviation. Dotted contours are from B^+ data, dashed contours are from B^- data.

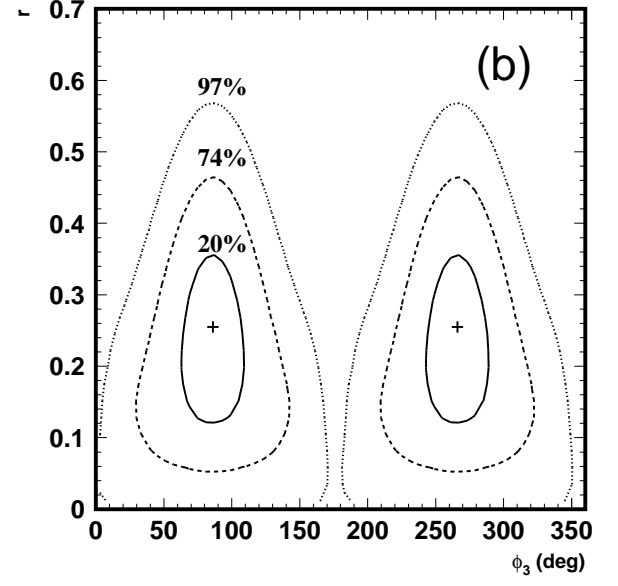
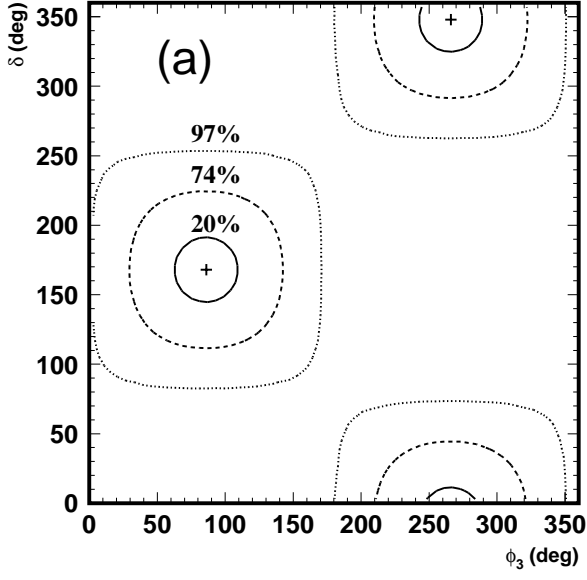


FIG. 10: Confidence regions for the pairs of parameters (a) (r, ϕ_3) and (b) (ϕ_3, δ) for the $B^\pm \rightarrow \tilde{D}K^\pm$ sample.

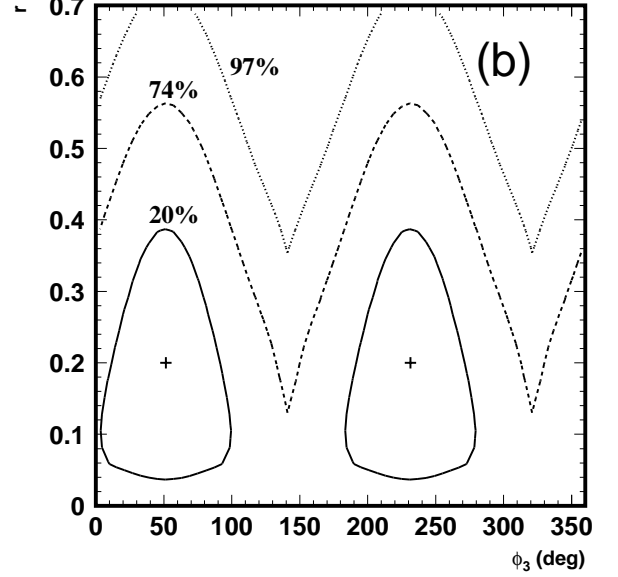
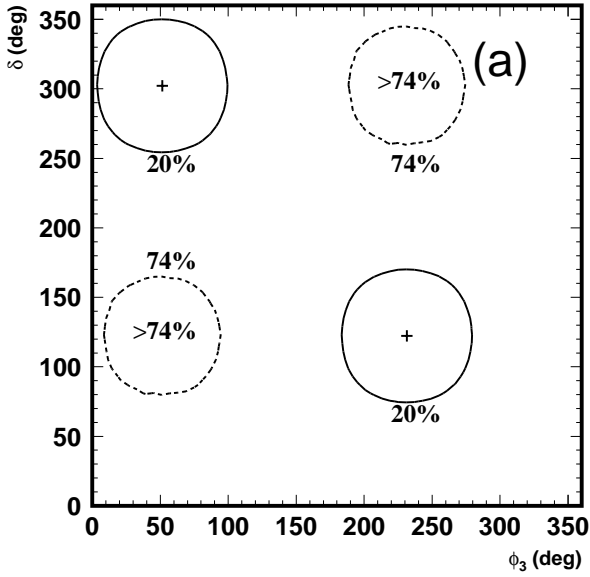


FIG. 11: Confidence regions for the pairs of parameters (a) (r, ϕ_3) and (b) (ϕ_3, δ) for the $B^\pm \rightarrow \tilde{D}^*K^\pm$ sample.